Two Modes of Change in Southern Ocean Productivity Over the Past Million Years

S. L. Jaccard *et al.*

Science **339**, 1419 (2013);
DOI: 10.1126/science.1227545

15. A. Shuler, G. Ekström, *J. Volcanol. Geotherm. Res.* **181**, 219 (2009).
16. G. Ekström, M. Nettles, A. M. Dziewonski, *Phys. Earth Planet. Inter.* **200-201**, 1 (2012).
17. H. Kanamori, J. W. Given, *J. Geophys. Res.* **87**, 5422 (1982).
18. H. Kanamori, J. W. Given, T. Lay, *J. Geophys. Res.* **89**, 1856 (1984).
19. H. S. Hasegawa, H. Kanamori, *Bull. Seismol. Soc. Am.* **77**, 1984 (1987).
20. E. E. Brodsky, E. Gordeev, H. Kanamori, *Geophys. Res. Lett.* **30**, 2236 (2003).
21. M. La Rocca *et al.*, *Bull. Seismol. Soc. Am.* **94**, 1850 (2004).
22. N. A. Pino, M. Ripepe, G. B. Cimini, *Geophys. Res. Lett.* **31**, L02605 (2004).
23. W. G. Pariseau, *Eng. Geol.* **16**, 111 (1980).
24. D. Petley, *Int. Water Power Dam Constr.* **63**, 27 (2011).
25. M. Peart, *Q. J. Eng. Geol.* **24**, 399 (1991).
26. Y.-J. Shang *et al.*, *Geomorphology* **54**, 225 (2003).
27. C.-H. Lin, H. Kumagai, M. Ando, T.-C. Shin, *Geophys. Res. Lett.* **37**, L22309 (2010).
28. M. Yamada, Y. Matsushi, M. Chigira, J. Mori, *Geophys. Res. Lett.* **39**, L13301 (2012).
29. V. M. Kotlyakov *et al.*, *Mater. Gliatsiologicheskikh Issledovanii* **95**, 221 (2003).
30. E. Eberhardt, D. Stead, J. S. Coggan, *Int. J. Rock Mech. Min. Sci.* **41**, 69 (2004).

Acknowledgments: We are grateful to C.-W. Lin, R.-J. Rau, S.-P. Lee, Hongey Chen, S.-H. Liu, and Y.-C. Tsang for help with analysis of landslides triggered by Typhoon Morakot; to E. Choi and M. Reitz for discussions on landslide mechanics; and to D. Petley for help and information on several of the landslide events reported here. Data are available in the supplementary materials. This research was supported by NSF Awards EAR-0824694, EAR-1150072, and EAR-1227083.

Supplementary Materials
www.sciencemag.org/cgi/content/full/339/6126/1416/DC1
Materials and Methods
Supplementary Text
Fig. S1
Table S1
References (*31*–*50*)

19 November 2012; accepted 30 January 2013
10.1126/science.1232887

Two Modes of Change in Southern Ocean Productivity Over the Past Million Years

S. L. Jaccard,[1] C. T. Hayes,[2,5] A. Martínez-García,[1] D. A. Hodell,[3] R. F. Anderson,[2,5] D. M. Sigman,[4] G. H. Haug[1]

Export of organic carbon from surface waters of the Antarctic Zone of the Southern Ocean decreased during the last ice age, coinciding with declining atmospheric carbon dioxide (CO_2) concentrations, signaling reduced exchange of CO_2 between the ocean interior and the atmosphere. In contrast, in the Subantarctic Zone, export production increased into ice ages coinciding with rising dust fluxes, thus suggesting iron fertilization of subantarctic phytoplankton. Here, a new high-resolution productivity record from the Antarctic Zone is compiled with parallel subantarctic data over the past million years. Together, they fit the view that the combination of these two modes of Southern Ocean change determines the temporal structure of the glacial-interglacial atmospheric CO_2 record, including during the interval of "lukewarm" interglacials between 450 and 800 thousand years ago.

Antarctic ice core measurements reveal that regional air temperatures and atmospheric CO_2 concentration (pCO_2) were tightly correlated over glacial-interglacial cycles of the past 800 thousand years (ky) (*1*). Many studies have inferred a dominant role for the Southern Ocean in modulating glacial-interglacial variability of atmospheric pCO_2 (*2*). The central role of the Southern Ocean is thought to reflect its leverage on the global efficiency of the biological pump, in which the production, sinking, and deep remineralization of organic matter sequesters carbon in the ocean interior, lowering atmospheric CO_2. Dense subsurface water masses outcrop in the Southern Ocean, providing exchange pathways between the deep ocean and the atmosphere. Vertical exchange of water causes deeply sequestered CO_2 and nutrients to be mixed to the surface, fueling high rates of phytoplankton productivity. Today, the Southern Ocean is the principal leak in the biological pump, because export production is inadequate to prevent the evasion of deeply sequestered carbon when waters are exposed to the atmosphere. The polar CO_2 leak can be directly inhibited during glacial stages by factors such as increased sea-ice cover (*3*) and/or changes in buoyancy forcing and convection (*4*, *5*). In addition, the glacial CO_2 reduction associated with these mechanisms would have been amplified by iron fertilization of the Subantarctic Zone (SAZ) of the Southern Ocean (*6*, *7*) and associated alkalinity feedbacks (*8*).

Export production records from the Antarctic Zone (AZ) have been used to trace changes in the rate of Southern Ocean overturning through time (*9*, *10*). However, these records only cover the last glacial cycle, restricting our understanding of the evolution of the Antarctic component of this two-mode system by which the Southern Ocean regulates the transfer of carbon between the ocean interior and the atmosphere over previous climatic cycles. Here, we report a high-resolution relative elemental concentration record from Ocean Drilling Program (ODP) site 1094 (53.2°S, 05.1°E; water depth 2850 m) (Fig. 1), which traces changes in AZ export production over the past million years (figs. S1 and S2). The time resolution achieved here rivals the measurement density typical for Antarctic ice-core records. These observations are complemented with reconstruction of ^{230}Th-normalized biogenic particle flux to the seafloor covering the last two glacial terminations (Fig. 2).

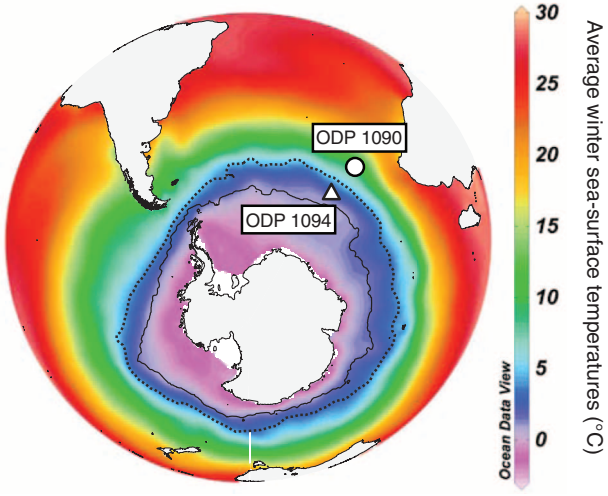

Fig. 1. Core locations shown on the January to March SST field. The black line delineates maximum winter sea-ice extent (using the 90% winter sea-ice concentration line) based on the Hadley Center sea-ice concentration data for 1978 to 2010 (*34*).

[1]Geological Institute, Department of Earth Sciences, ETH Zurich, Zurich, Switzerland. [2]Lamont-Doherty Earth Observatory, Columbia University, Palisades, NY, USA. [3]Godwin Laboratory for Paleoclimate Research, Department of Earth Sciences, University of Cambridge, Cambridge, UK. [4]Department of Geosciences, Princeton University, Princeton, NJ, USA. [5]Department of Earth and Environmental Sciences, Columbia University, New York, NY, USA.
*Corresponding author. E-mail: samuel.jaccard@erdw.ethz.ch

The pelagic sediment analyzed in this study is dominantly composed of diatomaceous opal and terrigenous detritus, the latter of which is mostly ice-rafted, with a minor contribution from aeolian material (*11*). Assuming that sedimentary iron (Fe) is of detrital origin, barium (Ba) abundance normalized to Fe yields an estimate of the sedimentary concentration of biogenic (or excess) Ba (bioBa), which serves as a tool to reconstruct changes in the integrated flux of organic matter to the sediment (*12*). Normalization by Fe assumes that the detrital fraction has not varied substantially in space and time, supported by provenance studies, indicating that the tephra-rich terrigenous material at this site is consistently derived from the South Sandwich volcanic arc, with negligible contribution from Bouvet Island and possibly the Antarctic Peninsula (*11*). Calcium (Ca) normalized to Fe indicates the sedimentary concentration of biogenic carbonate ($CaCO_3$). The records of Fe and Ti show almost identical trends in amplitude, but x-ray fluorescence signals are better for Fe, which is thus used for normalization. In these opal-rich sediments, elemental spectrum processing does not allow proper quantification of Al because of the overlapping Si peaks, precluding the use of Al as a normalizing agent.

The Ba/Fe record shows a strong climate-related signal (Fig. 3C), with high values during interglacials and lower values during cold stages. The Ba/Fe record is in good agreement with the ^{230}Th-normalized flux of bioBa (Fig. 2C), supporting the use of Ba/Fe to infer bioBa throughout the record. The large-scale Ba variations cannot be explained as the result of bacterially mediated sulfate reduction and associated diagenetic barite ($BaSO_4$) dissolution because no substantial sulfate reduction is observed in the interstitial water of the Pleistocene sediments of ODP site 1094 (*13*). Indeed, the ^{230}Th-normalized flux of bioBa is similar to that of opal and chlorophyll transformation products (chlorins) measured in the same sediment core (Fig. 2). Preservation of these independent paleo-productivity proxies is favored in different sedimentary environments. Whereas the preservation of bioBa can be compromised by reducing conditions, the preservation of organic matter in general, and chlorins in particular, is enhanced when oxygen content is low (*14*). The preservation of opal is unrelated to the redox state of sediments but is primarily driven by the total sedimentation rate (*15*). The correlation between opal fluxes and excess ^{231}Pa/^{230}Th at the same core site during the past 25 ky (*9*) and the correlation between opal fluxes and bioBa over the past 150 ky reported here indicate that the reconstructed opal fluxes most likely represent variable production by diatoms.

Consequently, the sedimentary Ba/Fe is interpreted to indicate lower bioBa accumulation and thus less export of organic matter from the surface ocean during cold periods, with the lowest bioBa concentrations coinciding almost exclusively with the glacial maxima, consistent with measurements elsewhere in the Southern Ocean, south of the polar frontal zone (*16*) (fig. S3). Sea ice has the potential to directly alter export production by blocking sunlight vital for phytoplankton to undertake photosynthesis; however, sea ice was only present at this site during the winters of glacial periods (*17*), not during the summer growing season. Rather, changes in export imply a reduced supply of nutrients to the surface ocean. Phytoplankton growth is inhibited by the lack of bioavailable Fe in most parts of the Southern Ocean. Vertical mixing and upwelling (rather than atmospheric fluxes) appear to dominate the supply of Fe to the Antarctic surface ocean at present (*18*). Thus, the glacial decrease in productivity may have been driven by a reduction in this deep-water–derived iron supply.

Although various physical mechanisms have been proposed for a reduction in this deep-water exposure, they all involve reduction of wind-driven upwelling, wintertime vertical mixing, or both (*4*, *5*, *19*). Upwelling could be lowered by weaker westerlies and/or by a more northerly position for them, whereas wintertime vertical mixing is sensitive to upper ocean density stratification. Various processes can affect this stratification, including upwelling, which strips away the freshwater cap (halocline) that maintains vertical stability.

Of the nitrate imported into the Antarctic surface today, only a portion derives from Ekman upwelling, with the remaining deriving from wintertime vertical mixing (*20*). Given that the data suggest many-fold lower export production during peak ice ages, we infer that these changes in productivity likely require both a reduction

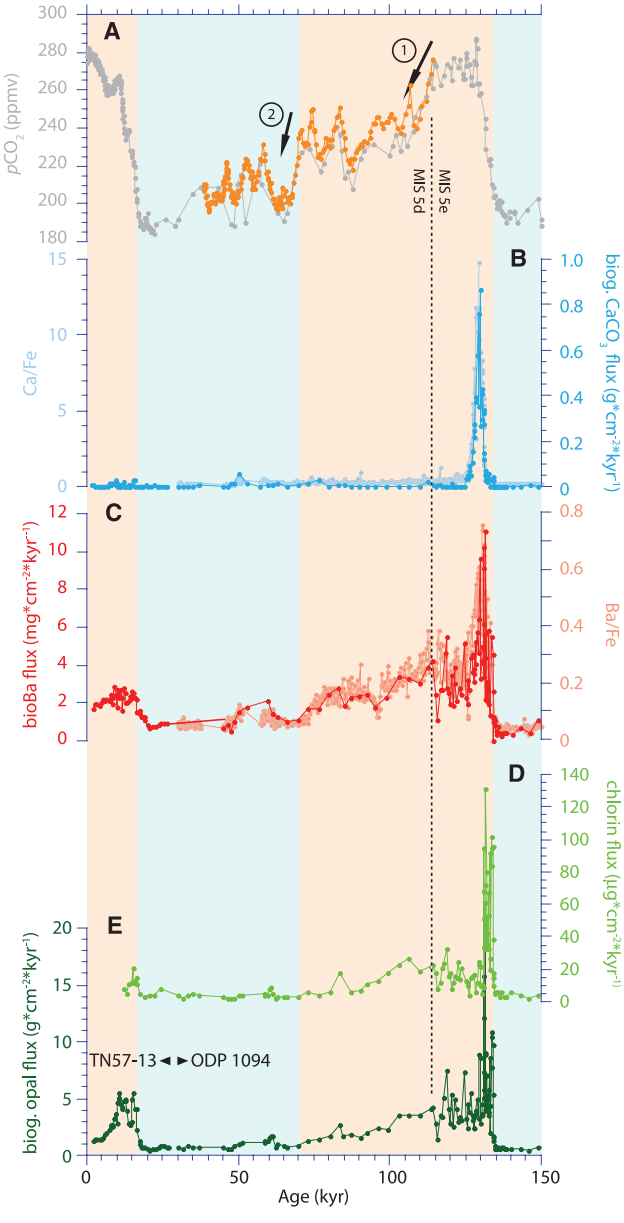

Fig. 2. Biogenic particle flux reconstructed by ^{230}Th normalization for four independent proxies covering the last two glacial terminations. Discrete measurements for the last 25 ky were performed on core TN-57-13PC. **(A)** Atmospheric pCO_2 (*1*, *35*). **(B)** Comparison between $CaCO_3$ flux and Ca/Fe. **(C)** Comparison between bioBa flux and Ba/Fe. **(D)** Chlorin flux. **(E)** Biogenic opal flux. Blue shadings highlight ice ages, whereas red shadings indicate interglacials. The two arrows highlight the two-step transition into ice ages.

in wind-driven upwelling and an increase in density stratification. This is important in that the latter change would affect deep-water formation, through which the Antarctic has its greatest direct leverage on atmospheric CO_2 (*21*, *22*).

Upon glacial terminations, large pulses of export production coincide with prominent increases in atmospheric CO_2 concentrations reconstructed from Antarctic ice cores (Figs. 2 and 3). Flux determinations of three independent export production proxies suggest that the export of organic matter increased by more than an order of magnitude across the two last climate transitions (Fig. 2). Reconstruction of past silicon and nitrogen dynamics suggests that relative nutrient utilization did not rise sharply at the last glacial termination (*23*), such that the rise in bioBa and opal fluxes was a response to a large increase in the nutrient supply to the euphotic zone. These increases in export were accompanied by summer sea surface temperature (SST) overshoots and abrupt disappearances of winter sea ice (*17*). Summer SSTs increased by more than 4°C in less than 5 ky for the last five glacial terminations (*17*). Although the sequence of deglacial events remains to be resolved (*9*), the systematic and repeated glacial-to-interglacial rises in biogenic flux (Fig. 3) point to a robust pattern of enhanced Southern Ocean overturning during interglacials.

Moreover, we show that these glacial-to-interglacial export production increases were accompanied by short-lived $CaCO_3$ spikes in these otherwise carbonate-poor sediments (Fig. 3D). We note that the preservation spike observed for the last glacial termination is muted at this site, for reasons that remain unclear. The near absence of $CaCO_3$ in most of the record suggests that seafloor preservation of the $CaCO_3$ rain regulated the bimodal character of the record. Although intervals with higher sedimentary $CaCO_3$ concentrations could in principle reflect increased local $CaCO_3$ export, the abrupt increases and the transient nature of the $CaCO_3$ spikes compared with export production proxies argue instead for a transient deepening of the lysocline, as expected if CO_2 was lost from deep waters at this time.

The decrease in deep-water exposure after peak interglacial conditions, indicated by declining export production, leads to pCO_2 reduction, and this mechanism appears to apply in particular to the early stages of glaciation. As a general rule, elevated Antarctic export occurs during the peak interglacials, giving way to a major decline in the early stages of glaciation (Fig. 3 C), coinciding with the first half of the CO_2 decline into each glacial period, 40 to 50 parts per million (ppm) (Fig. 3A, reaching ~225 ppm). Remarkably, this is a similar, if slightly greater, reduction than is estimated by numerical models for the CO_2 decline that should result from a strong reduction in Antarctic overturning (*21*, *24*). Although further declines in Antarctic export production occur later in the glacial progression (Fig. 3C), the associated CO_2 reduction associated with this mechanism should have nearly saturated (*2*). However, based on data from ODP Site 1090 in the SAZ to the north of ODP Site 1094, it appears that the later stages of glaciation and climate cross a threshold at which the SAZ undergoes a dramatic rise in productivity (Fig. 3F) (*6*, *25*) coincident with increased dust-borne iron supply to the SAZ from continental regions upstream in the westerly wind field (Fig. 3E) (*7*). Iron fertilization in the SAZ would have permitted biological productivity in this region to sequester additional regenerated

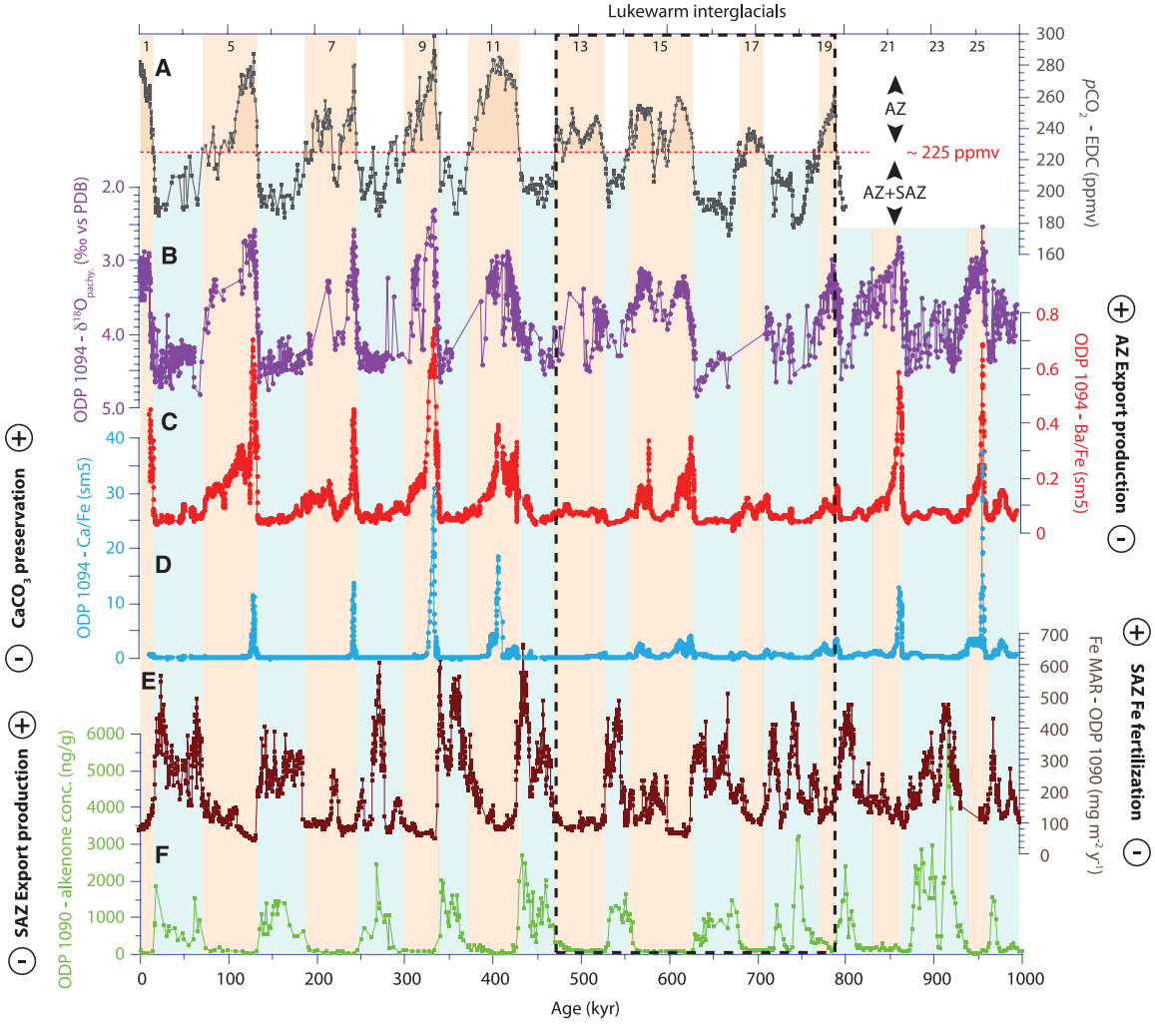

Fig. 3. Records of **(A)** atmospheric pCO_2 (*1*), **(B)** ODP 1094 planktic foraminifera $\delta^{18}O$ (*36*, *37*), **(C)** ODP 1094 Ba/Fe (data smoothed by a five-point running mean), **(D)** ODP 1094 Ca/Fe (data smoothed by a five-point running mean), **(E)** Fe flux to subantarctic core ODP 1090 (*7*), and **(F)** ODP 1090 sedimentary alkenone concentration (*25*) covering the past 1 million years. Red and blue shadings highlight intervals where AZ/SAZ processes, respectively, are dominantly controlling the partitioning of CO_2 between the ocean interior and the atmosphere. During glacial inceptions, the first half of the pCO_2 reduction is essentially accomplished by decreasing vertical mixing and upwelling in the AZ (red shading). The second portion of the pCO_2 reduction (blue shadings), initiated around 225 parts per million by volume (ppmv), is achieved by enhancing carbon sequestration resulting from increased Fe fertilization in the SAZ, thereby leading the climate system to reach full glacial conditions.

carbon in the abyssal ocean, which would have further lowered atmospheric CO_2 (*16*, *26*). It is again notable that numerical model simulations of subantarctic iron fertilization predict roughly the observed CO_2 declines of ~40 ppm that occur later in the glacial progressions (*21*, *24*, *26*). In the modern ocean, there is upper ocean mixing across the fronts separating the AZ and the SAZ (*27*). Thus, during peak ice conditions, iron fertilization in the SAZ may have further depleted the AZ of surface nutrients, contributing to the continued decline of AZ export production to its glacial minimum. In any case, it is a remarkable characteristic of the two records that the SAZ biological response begins when AZ productivity has reached the lower half of its range (Fig. 3, C and F), with relatively little correlated variation between the AZ and SAZ (Fig. 4), and that the major changes in each correspond to roughly half of the observed CO_2 variation (Fig. 4). In summary, the paleoceanographic records from both the AZ and SAZ merge with the numerical model estimates of the Southern Ocean to provide a coherent two-part Southern Ocean mechanism for the amplitude and timing of glacial interglacial CO_2 change.

The potential for these two modes of the Southern Ocean to have different roles in glacial-interglacial CO_2 change, first recognized in the context of the last glacial cycle (*2*, *16*), is bolstered by the data reported here for the period of the "lukewarm" interglacials [marine isotope stage (MIS) 13 to 19]. The lukewarm interglacials are characterized by reduced amplitude of the ice-core δD and CO_2 records (Fig. 3) and a general decrease in global interglacial temperatures that appears to be more pronounced in Southern Ocean SST records (*28*). Given the potential dependencies of westerly wind position (*29*) and polar ocean water-column stability (*30*) on global temperature, the muting of the pCO_2 increase during the lukewarm interglacials might have been linked to a reduced dynamic range of Antarctic overturning, with the abyssal ocean thereby maintaining a larger reservoir of regenerated carbon than in more recent interglacials (*31*). This hypothesis is supported by the Antarctic Ba/Fe record (Fig. 3C), which shows markedly reduced amplitude for the Ba/Fe maxima associated with the lukewarm interglacials (Fig. 4, squares with open circles along the *x* axis). Furthermore, this interval also generally has reduced deglacial $CaCO_3$ peaks (Fig. 3D), which would suggest that proportionally less CO_2 was released from the deep ocean. The expression of interglacials in the SAZ record is indistinguishable between the period containing the lukewarm interglacials and the rest of the record (Figs. 3 and 4) (*7*, *25*), suggesting that the cessation of SAZ iron fertilization occurred during the lukewarms as in other interglacials.

In contrast to the lukewarm interglacials, MIS 21 and 25 were characterized by full-amplitude export production peaks in the AZ accompanied by large $CaCO_3$ preservation events, suggesting an increase in upwelling and deep-ocean CO_2 release during glacial terminations X and XI (Fig. 3), consistent with planktic foraminiferal pH estimates that suggest that both interglacials had pCO_2 values as high as recent interglacials (*32*). This observation further argues that the subsequent lukewarm interglacials represented a distinct period. Our observations thus indicate a strong coupling between Antarctic deep-to-surface exchange and the magnitude of the CO_2 release from the ocean interior, which is consistent with observed changes in atmospheric pCO_2 even beyond the interval covered by the Antarctic ice-core records.

There is much uncertainty and debate regarding the response of Southern Ocean overturning to ongoing global warming, as well to its impact on the oceanic uptake of anthropogenic CO_2 (*33*). The paleoclimate data reported here argue strongly for a robust sensitivity of Antarctic overturning to global climate, in which overturning increases under warmer conditions. As the physical mechanism of this coupling is not yet clear, one cannot be confident that it will apply on the decadal to centennial scale and under the specific conditions of anthropogenic global warming. Nonetheless, the finding of stronger overturning under warmer climates, taken at face value, suggests a similar sense of change for the warmer future ocean.

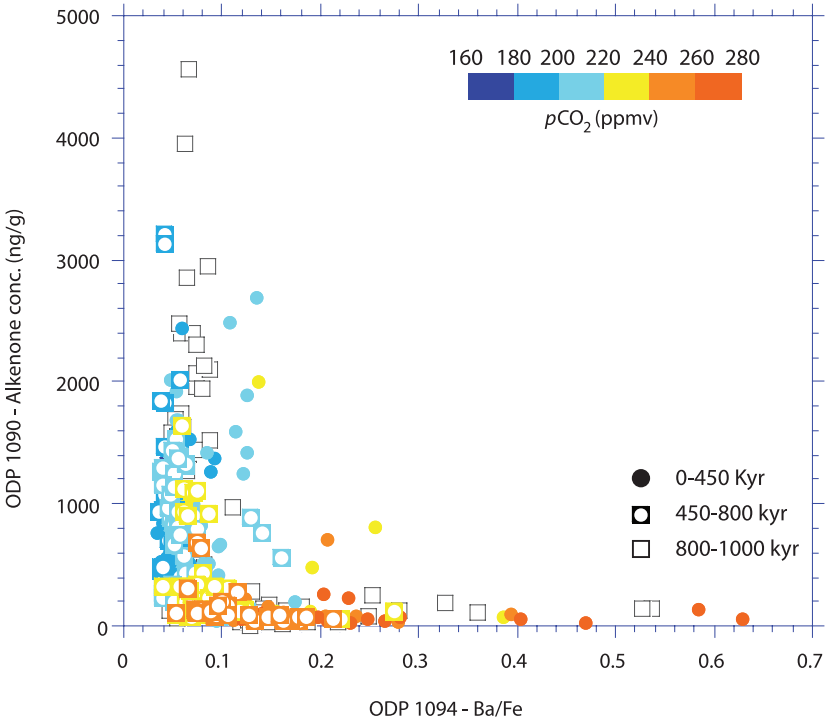

Fig. 4. Comparison between ODP 1094 Ba/Fe and ODP 1090 sedimentary alkenone concentration (*25*). Symbol color indicates pCO_2. Filled circles illustrate the period 0 to 450 ky, filled squares the lukewarm interval (450 to 800 ky), and the open squares the interval 800 to 1000 ky, for which ice core pCO_2 data do not yet exist.

References

1. D. Lüthi *et al.*, *Nature* **453**, 379 (2008).
2. D. M. Sigman, M. P. Hain, G. H. Haug, *Nature* **466**, 47 (2010).
3. R. F. Keeling, B. B. Stephens, *Paleoceanography* **16**, 112 (2001).
4. J. J. R. Toggweiler, J. L. Russell, S. Carson, *Paleoceanography* **21**, PA2005 (2006).
5. A. J. Watson, A. C. Naveira Garabato, *Tellus* **58B**, 73 (2006).
6. N. Kumar *et al.*, *Nature* **378**, 675 (1995).
7. A. Martínez-Garcia *et al.*, *Nature* **476**, 312 (2011).
8. R. Keir, *Paleoceanography* **3**, 413 (1988).
9. R. F. Anderson *et al.*, *Science* **323**, 1443 (2009).
10. R. François *et al.*, *Nature* **389**, 929 (1997).
11. S. H. H. Nielsen, D. A. Hodell, G. Kamenov, T. Guilderson, M. R. Perfit, *Geochem. Geophys. Geosyst.* **8**, Q12005 (2007).
12. J. Dymond, E. Suess, M. Lyle, *Paleoceanography* **7**, 163 (1992).
13. R. Gersonde, D. A. Hodell, P. Blum, Eds., *Proceedings of the Ocean Drilling Program, Initial Results, Leg 177* (Ocean Drilling Program, College Station, TX, 1999), chap. 9.
14. K. A. F. Zonneveld *et al.*, *Biogeosciences* **7**, 483 (2010).
15. F. L. Sayles, W. R. Martin, Z. Chase, R. F. Anderson, *Deep Sea Res. Part II Top. Stud. Oceanogr.* **48**, 4323 (2001).
16. K. E. Kohfeld, C. Le Quéré, S. P. Harrison, R. F. Anderson, *Science* **308**, 74 (2005).
17. A. Schneider-Mor *et al.*, *Geophys. Res. Lett.* **32**, L10704 (2005).
18. N. Lefèvre, A. J. Watson, *Global Biogeochem. Cycles* **13**, 727 (1999).
19. A. E. S. Kemp, I. Grigorov, R. B. Pearce, A. C. Naveira Garabato, *Quat. Sci. Rev.* **29**, 1993 (2010).
20. M. J. Lourey, T. W. Trull, *J. Geophys. Res.* **106**, 31463 (2001).
21. M. P. Hain, D. M. Sigman, G. H. Haug, *Global Biogeochem. Cycles* **24**, GB4023 (2010).
22. I. Marinov *et al.*, *Global Biogeochem. Cycles* **22**, GB3007 (2008).
23. M. G. Horn, C. P. Beucher, R. S. Robinson, M. A. Brzezinski, *Earth Planet. Sci. Lett.* **310**, 334 (2011).
24. V. Brovkin, A. Ganopolski, D. Archer, S. Rahmstorf, *Paleoceanography* **22**, PA4202 (2007).
25. A. Martinez-Garcia *et al.*, *Paleoceanography* **24**, PA1207 (2009).
26. A. J. Watson, D. C. E. Bakker, A. J. Ridgwell, P. W. Boyd, C. S. Law, *Nature* **407**, 730 (2000).

27. P. J. DiFiore *et al.*, *J. Geophys. Res.* **111**, C08016 (2006).
28. N. Lang, E. W. Wolff, *Clim. Past* **7**, 361 (2011).
29. J. Russell, K. W. Dixon, A. Gnanadesikan, R. J. Stouffer, J. R. Toggweiler, *J. Clim.* **19**, 6382 (2006).
30. A. M. de Boer, D. M. Sigman, J. R. Toggweiler, J. L. Russell, *Paleoceanography* **22**, PA2210 (2007).
31. S. L. Jaccard, E. D. Galbraith, D. M. Sigman, G. H. Haug, *Quat. Sci. Rev.* **29**, 206 (2010).
32. B. Hönisch, N. G. Hemming, D. Archer, M. Siddall, J. F. McManus, *Science* **324**, 1551 (2009).
33. C. Le Quéré *et al.*, *Nat. Geosci.* **2**, 831 (2009).
34. N. A. Rayner *et al.*, *J. Geophys. Res.* **108**, (D14), 4407 (2003).
35. B. Bereiter *et al.*, *Proc. Natl. Acad. Sci. U.S.A.* **109**, 9755 (2012).
36. D. A. Hodell *et al.*, in *Proceedings of the Ocean Drilling Program, Scientific Results,* R. Gersonde, D. A. Hodell, P. Blum, Eds. (Ocean Drilling Program, College Station, TX, 2003), vol. 177, chap. 9.
37. H. F. Kleiven, E. Jansen, in *Proceedings of the Ocean Drilling Program, Scientific Results,* R. Gersonde, D. A. Hodell, P. Blum, Eds. (Ocean Drilling Program, College Station, TX, 2003), vol. 177, chap. 12.

Acknowledgments: We thank S. Stefer for performing the XRF scanning measurements at the University of Bremen. We also acknowledge the Integrated Ocean Drilling Program for providing the samples used in this study and U. Röhl, A. Wülbers and W. Hale for their support at the Bremen IODP core repository. This research used data acquired at the XRF Core Scanner Laboratory at the MARUM – Center for Marine Environmental Sciences, University of Bremen. We further thank E. D. Galbraith as well as three anonymous reviewers, whose comments improved the manuscript. Financial support for this work was provided by the Swiss National Science Foundation (SNSF), the Deutsche Forschungsgemeinschaft (DFG), the U.S. National Science Foundation, and the Comer Science and Education Foundation.

Supplementary Materials
www.sciencemag.org/cgi/content/full/339/6126/1419/DC1
Materials and Methods
Figs. S1 to S3
References

17 July 2012; accepted 16 January 2013
10.1126/science.1227545

Emergence and Diversification of Fly Pigmentation Through Evolution of a Gene Regulatory Module

Laurent Arnoult,* Kathy F. Y. Su,* Diogo Manoel,* Caroline Minervino, Justine Magriña, Nicolas Gompel,† Benjamin Prud'homme†

The typical pattern of morphological evolution associated with the radiation of a group of related species is the emergence of a novel trait and its subsequent diversification. Yet the genetic mechanisms associated with these two evolutionary steps are poorly characterized. Here, we show that a spot of dark pigment on fly wings emerged from the assembly of a novel gene regulatory module in which a set of pigmentation genes evolved to respond to a common transcriptional regulator determining their spatial distribution. The primitive wing spot pattern subsequently diversified through changes in the expression pattern of this regulator. These results suggest that the genetic changes underlying the emergence and diversification of wing pigmentation patterns are partitioned within genetic networks.

Whether emergence and diversification of morphological traits both occur through changes at the same tier of a gene regulatory network is currently an open question in evolutionary biology. We addressed this question by studying a wing pigmentation pattern that evolved recently in the *Drosophila melanogaster* group. Although this male-specific wing spot assumes different shapes, colors, and intensities among species (Fig. 1 and fig. S1), phylogenetic reconstruction indicates that it emerged only once in this lineage and subsequently diversified (*1*).

We examined the expression pattern of *yellow* (*y*), a gene required for the production of black pigment patterns, including the wing spot (*2*). Yellow distribution in the wing of pupae or young adults precisely foreshadows the adult pigmentation pattern in the various species we studied (Fig. 1), suggesting that understanding the evolution of *y* expression patterns would illuminate how the wing spot appeared and diversified. The wing spot expression pattern of *y* in *D. biarmipes*, a wing-spotted species, is encoded by an evolutionarily derived cis-regulatory element (CRE) of the *yellow* locus (*2*), the *spot* CRE [hereafter referred to as *y spot*^{bia675} (*3*)]. Therefore, to decipher how the wing spot expression of *y* is spatially regulated, we sought to identify the transcription factors controlling the localized activity of the *y spot*^{bia196} CRE, a minimal version of *y spot*^{bia675} CRE with a similar activity (*2*).

The *y spot*^{bia196} CRE is functional in *D. melanogaster* wing, and we used its transcriptional activity as a readout in an RNA interference (RNAi) screen targeting selected genes to identify its transcriptional activators. With this functional screen of the ~350 transcription factors expressed in a *D. melanogaster* late pupal wing (table S1), we identified a handful of candidates (fig. S2). Among five candidate activators, *Distal-less* (*Dll*) first caught our attention because of its well-defined role in wing patterning. When *Dll* is down-regulated, the activity of the *y spot*^{bia196} CRE is severely affected (Fig. 2, A and B, and fig. S2C). Reciprocally, we overexpressed Dll throughout the wing, which resulted in an increase and an expansion of the *y spot*^{bia196} activity (Fig. 2C). These genetic manipulations reveal that *Dll* is both necessary and sufficient to control the activity of the *y spot*^{bia196} CRE in a *D. melanogaster* context.

By scanning the *spot*^{bia196} CRE, we identified several putative Dll binding sites. We tested the ability of Dll to bind these sites in vitro (fig. S3, A and B) and, thus, discovered that Dll can physically interact with four of them. Mutations of these sites preventing Dll binding in vitro also impaired the activity of the *y spot*^{bia196} CRE in vivo (Fig. 2D and fig. S3C). Of note, the same mutations also abolish the *y spot*^{bia196} response to Dll overexpression (fig. S3D). Together, these results indicate that the *y spot*^{bia196} CRE contains multiple binding sites for Dll and suggest that the evolution of a regulatory link between Dll and *yellow* was essential for the emergence of the wing spot.

The results obtained in *D. melanogaster* stimulated the investigation of the role of *Distal-less* in wing pigmentation pattern formation in *D. biarmipes*. We established a loss-of-function assay based on the expression of artificial short hairpin microRNA (shRNA) (*4*) and validated the system in *D. biarmipes* by silencing *yellow* in the pupal wing (fig. S5, A and C), which phenocopies a *y* mutant. The down-regulation of Dll, using the same shRNA approach, resulted in a dramatic reduction of the pigmentation spot (Fig. 3, A and B, and fig. S4, A to D); however, the uniform gray shading of the wing was not affected. Reciprocally, the overexpression of Dll throughout the wing yielded ectopic pigmentation across the wing (Fig. 3, A and C, and fig. S4, E to G and J). Together, these results establish that *Dll* plays an essential role in wing spot formation in *D. biarmipes*.

To test the specificity of the effect of *Dll* on wing spot pattern formation in *D. biarmipes*, we first examined the other transcription factors identified in our RNAi screen. Contrary to *Dll*, none of the candidates that we overexpressed across the wing were sufficient to induce ectopic pigmentation (fig. S4, H to M). These results highlight the specific role of *Dll* in the wing pigmentation spot formation. Second, we ectopically expressed *Dll* in the wing of the nonspotted species *D. ananassae*, a species with an ancestral pattern predating the wing spot evolution (Fig. 1) (*1*). In this species, *Dll* overexpression had no effect on wing pigmentation (fig. S6G), suggesting that the regulatory interactions between Dll and downstream pigmentation genes are absent. Consistent

Aix-Marseille Université, CNRS, UMR 7288, Institut de Biologie du Développement de Marseille-Luminy, 13288 Marseille cedex 9, France.

*These authors contributed equally to this work.
†Corresponding author. E-mail: nicolas.gompel@univ-amu.fr (N.G.); benjamin.prudhomme@univ-amu.fr (B.P.)